



Magnetoelectricity in vertically aligned nanocomposites: Past, present, and future

Min Gao,* Yaodong Yang, Wei-Feng Rao, and D. Viehland

Vertically aligned magnetoelectric nanocomposites (ME VANs) self-assembled from piezoelectric perovskite and magnetostrictive spinel phases are appealing due to their unique pillar-array-like morphologies and enhanced ME properties. The strain-mediated ME effect leads to various field-dependent characteristics that are tunable, which provides application pathways in microelectronics. The microstructure formation mechanisms of ME VANs have been explored by phase field simulations. Several effective approaches to modify and improve the ME properties of VANs are discussed, including orientations, deposition conditions, and substrate types. Potential applications are also discussed, such as field tunable “adaptive” microelectronics and multistate memory devices.

History and background

The magnetoelectric (ME) effect refers to the interaction between ferroelectric and ferromagnetic order parameters in a material, which allows control of the magnetization (M) by electric fields (E), or conversely control the polarization (P) by magnetic fields (H).^{1–5} Therefore, ME materials have potential in various electronic devices such as sensors, gyrators, and memory devices.^{4–8} The ME coefficient and converse ME coefficient can be defined by Equations 1 and 2, respectively:

$$\alpha_{ME} = \frac{dD}{dH} \quad (1)$$

$$\alpha_{CME} = \frac{dM}{dE}, \quad (2)$$

where D is the dielectric displacement.^{1,4} This definition can be explained by free energy polynomial expressions using Landau theory.^{1,9–12}

Single-phase ME materials have low ME coefficients. Consequently, much effort has focused on developing ME composites of piezoelectric and magnetostrictive components,

where the two phases are coupled together through strain that produces enhanced ME coefficients, via product tensor properties.^{1,2,4} In order to foster integration in microelectronics, ME composites have been miniaturized to the nanoscale.^{13–15} Among the approaches, ME vertically aligned nanocomposites (VANs) are appealing due to their unique phase distribution morphologies, and enhanced ME properties.^{1,15–17} These ME VANs are self-assembled from piezoelectric perovskite and magnetostrictive spinel phases by minimization of the strain energy and surface/interfacial energy.^{17–20} **Figure 1a** shows a schematic that demonstrates the morphology difference between traditional multilayer thin films and ME VANs.¹⁶ Instead of a classic layer-by-layer structure, ME VANs of two phases are usually nanopillars of one phase self-assembled into a continuous matrix of the other phase. Increased interfacial surface area for the ME VANs and a weaker substrate-clamping effect lead to an enhanced strain-mediated ME effect.^{17,21} However, because the magnetostrictive nanopillars that penetrate the piezoelectric matrix usually have a much lower resistivity, leakage problems have been reported.²² To overcome this limitation, a buried ME VAN structure has

Min Gao, College of Materials Science and Engineering, Fuzhou University, China; and Department of Materials Science and Engineering, Virginia Polytechnic Institute and State University, USA; gaom@fzu.edu.cn

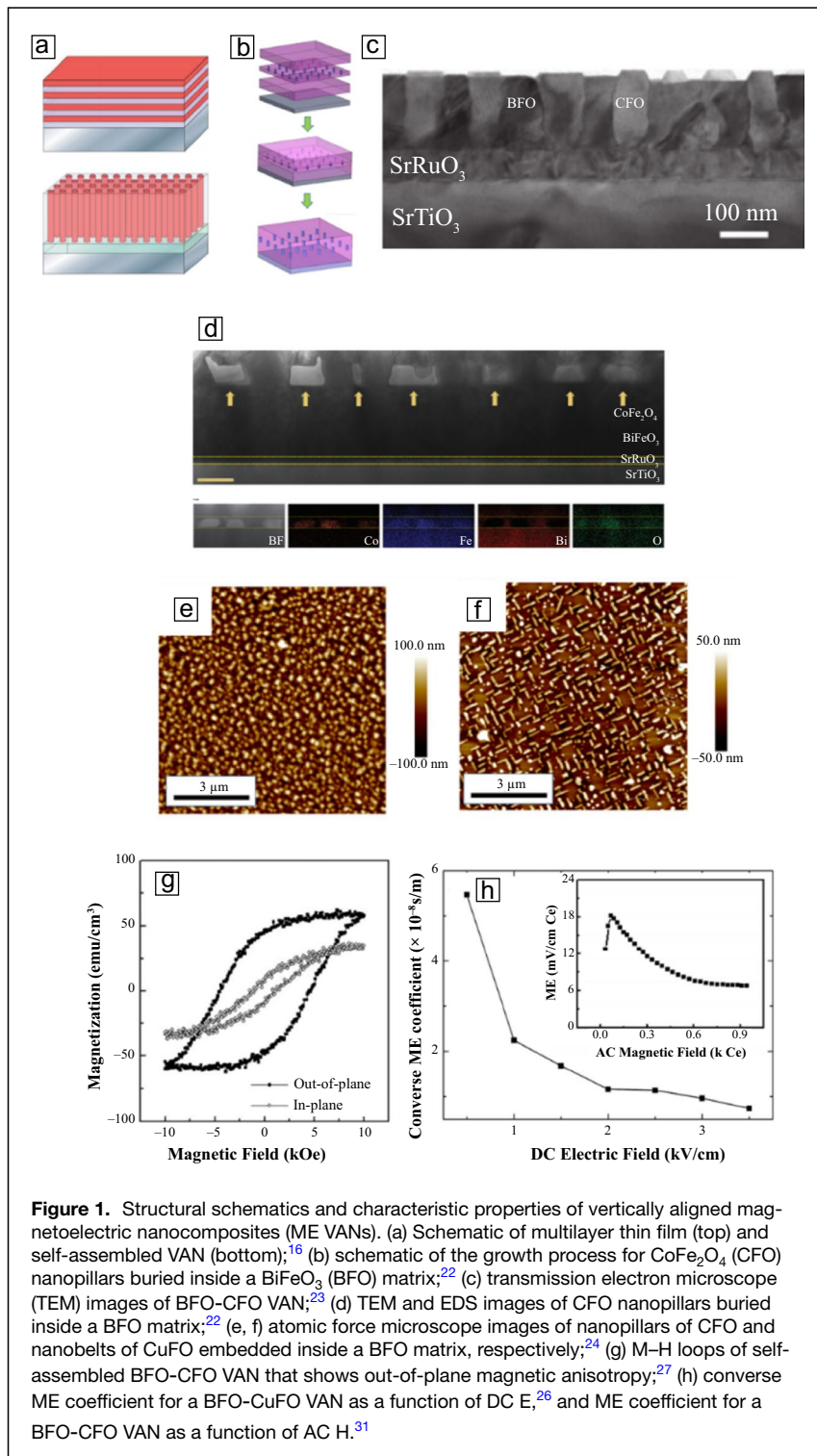
Yaodong Yang, School of Mechanical and Automotive Engineering, Qilu University of Technology, Shandong Academy of Sciences, China; yaodongy@qlu.edu.cn

Wei-Feng Rao, School of Mechanical and Automotive Engineering, Qilu University of Technology, Shandong Academy of Sciences, China; and State Key Laboratory of Biobased Material and Green Papermaking, Qilu University of Technology, Shandong Academy of Sciences, China; wfrao@qlu.edu.cn

D. Viehland, Department of Materials Science and Engineering, Virginia Polytechnic Institute and State University, USA; dviehlan@vt.edu

*Corresponding author

doi:10.1557/s43577-021-00027-1



been proposed, as shown in Figure 1b, where ME VANs are sandwiched between two additional thin piezoelectric layers.²² Since the magnetostrictive nanopillars are completely covered, the leakage current could be significantly reduced.²² Figure 1c, d show transmission electron microscope (TEM) images for normal and buried BiFeO_3 - CoFe_2O_4 (BFO-CFO) VANs, respectively.^{22,23}

An important feature for ME VANs is the adjustable morphology-related properties.^{2,3,20} For example, Figure 1e, f show the surface morphologies of BFO-CFO VAN and BiFeO_3 - CuFe_2O_4 (BFO-CuFO) VAN on (001) oriented $\text{Pb}(\text{Mg}_{1/3}\text{Nb}_{2/3})\text{O}_3$ - PbTiO_3 (PMN-PT) single-crystal substrates, respectively.²⁴ The CFO nanopillars lay vertical to the substrate, whereas the CuFO forms nanobelts that are horizontal to the substrate, but perpendicular to each other.²⁴ The vertically aligned ferromagnetic nanopillars have an out-of-plane magnetic anisotropy (see Figure 1g), whereas the in-plane perpendicular ferromagnetic nanobelts exhibit a fourfold in-plane magnetic anisotropy. By control of the morphology of ME VANs, one can then tune the magnetic anisotropy from out-of-plane to in-plane direction.^{25–28} Furthermore, ME VANs have enhanced ME properties, compared to ME heterostructural thin films.^{5,22,29,30} This yields field tunable ME properties with either E or H (see Figure 1h), offering ME VANs potential for E-tunable inductors and H-tunable capacitors.^{26,31}

Since the first report of BiTiO_3 - CoFe_2O_4 (BTO-CFO) VANs in 2004, many other VAN systems with different combinations of perovskite and spinel phases have been reported, such as PbTiO_3 - CoFe_2O_4 (PTO-CFO),^{32,33} $\text{Pb}(\text{Ti,Zr})\text{O}_3$ - CoFe_2O_4 (PZT-CFO),^{34,35} and BiFeO_3 - NiFe_2O_4 (BFO-NFO).³⁶ To provide a universal and distinct understanding of ME VANs, the BFO-CFO based VAN system is chosen as an example in this article, whereas ME VANs with other compositions and the material selection strategies can be found in some recent reviews.^{2,5,7,14,17,29} Pulsed laser deposition (PLD) is a reliable method for VAN growths because it offers high-quality epitaxial growth for complex oxides, which facilitate self-assembly.

Recently, a unique method called fast switching PLD (FSPLD) has been reported, where multiple single-phase targets can be frequently switched during the deposition process and VANs with different components and volume ratio can be controlled. By utilizing FSPLD, there is no need to fabricate targets of different components and volume fractions.^{24,26,28,37,38} If the

target is switching fast enough, the thickness of individual phase layers will be so thin that the multilayer thin films will self-assemble into two-phase mixed VAN structure because the latter has lower formation energy.^{28,37,38} By choosing various targets and controlling the ablation time, one can conveniently adjust the components and volume fractions in VANs. For potential large-scale fabrication requirements, sputtering has also been studied.^{5,21,39,40}

In the following sections, we will focus on (1) the phase distribution in ME VANs; (2) diverse approaches to adjust the morphology and ME performances; and (3) the potential in various microelectronic applications.

Simulating the phase distribution morphology of ME VANs

Observation of the phase distribution in ME VANs is crucial to understand their ME properties. Although it is difficult to observe *in situ* the dynamics of phase distribution and the formation of vertically aligned interfaces, appropriate simulation methods can provide key insights.

The formation of ME VANs is an energy-reducing process involving the simultaneous evolution of structural, polar, and magnetic order parameters. In order to correctly describe the thermodynamics and kinetics of a system, the total free energy has to include at least (1) the local chemical free energies characterizing the stress-free crystal lattices of both inclusion and matrix phases as functions of composition, and temperature; (2) the interfacial energies describing the short-ranged interactions across interfaces separating the film and substrate, the inclusion and matrix phases, and the symmetrically equivalent structural/polar/magnetic variants/domains; and (3) the long-ranged elastic, electrostatic and magnetostatic energies caused by the highly heterogeneous distribution of structural, polar, and magnetic order parameters, and their reactions to externally applied fields. Therefore, simulating the microstructure formation and corresponding properties of ME VANs is a challenging task beyond the capabilities of most simulation methods.

The phase-field method (PF) is, however, very suitable for this task because it can explicitly consider all energies contributions. For example, the local chemical energy is usually described in PF by Landau polynomials fitted to available material constants, physical properties, and phase diagrams; and the elastic energy introduced by lattice-misfit inclusions of arbitrary shapes can be exactly calculated based on Khachaturyan–Shatalov theory.^{41,42} Furthermore, a generalized equivalency principle in a unified PF framework has been developed to exactly solve the strain, polarization, and magnetization fields in magneto-electro-elastic solids with arbitrary microstructures under applied loadings.⁴³ No *a priori* assumption is needed in PF about the evolution of microstructure: the movements of phase/domain boundaries/interfaces are described by the temporal and spatial changes of order parameters that are directly driven by the energy reduction.

PF is especially suitable for investigating self-assembling microstructure formation. This method has been used to systematically investigate the effects of lattice misfits, elastic properties, and relative fractions of constituent phases, and film thickness on the morphology of self-assembling nanostructures in constrained films.^{44,45} Figure 2a shows the microstructure of films obtained by simulating the pseudo-spinodal decomposition in PF, demonstrating the possibility of forming a vertically aligned nanoscale morphology by adjusting the energy competition among different origins (e.g., interfacial versus elastic energies).⁴⁶

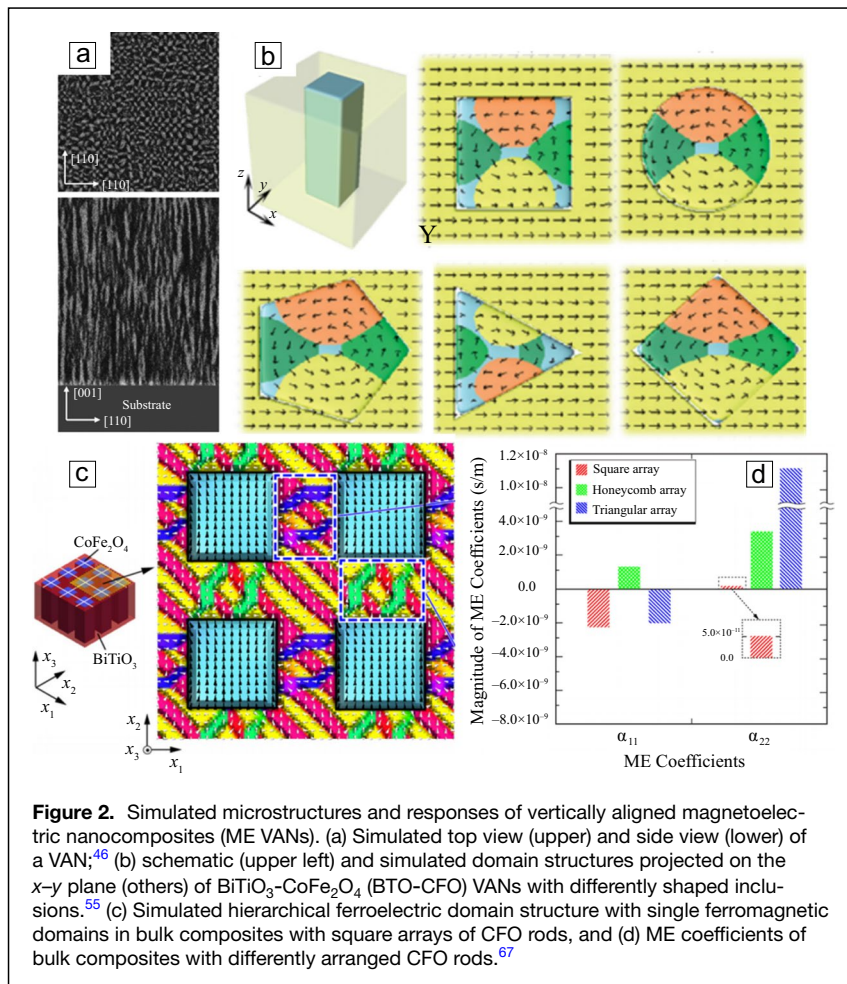
Understanding what controls ME VANs, and rich approaches to adjustments via film growth

It is critical to understand the underlying parameters controlling ME couplings in VANs. PF simulation reveals several important factors, such as the distribution of each phase, the size of each phase, and the strain effect in ME VANs. Indeed, functional properties in VANs are often strongly tied to interface, defect, and strain at the vertical interfaces in a variety of VANs.⁴⁷ Meanwhile, advanced probe microscopes have been employed to directly observe and verify these phase/polarization distributions (with/without fields) of each domain at the micron/nanoscale.^{48–50} It has been reported that the pillar size plays a critical role in controlling ME coupling in BTO-CFO VANs as it is determined by the competition between the vertical interface coupling effect and the bulk volume conservation effect.^{51,52} Moreover, experiments have also been widely performed to improve the phase distribution morphologies and to enhance the properties of ME VANs. In addition to various piezoelectric and magnetostrictive phase combinations,^{16,20,28,32–36,53} studies (theory and experiments) reveal that the VAN morphology and properties can be controlled by shape and orientations,^{3,20,25,54,55} deposition conditions,^{19,56–59} and substrate constraints.^{24,60–63}

Shape and orientation effects

As a numerical tool specializing in mesoscale phenomena, PF is powerful in understanding domain-level mechanisms/effects in nanostructured composites. It has been employed to study the polarization distributions in ME VANs comprised of triangle, square, circle, or polygon-shaped BTO rods embedded in a CFO matrix.⁵⁵ Results show that the polarization domain structure changes from normal multidomain states to single-vortex structures, as the sizes of rods are decreased from ~100 to ~10 nm (see Figure 2b).⁵⁵ The geometrical shapes and the aspect ratio of rods, as well as the magnetization orientation in the magnetic matrix, can strongly affect the ferroelectric domain structures, and phase distributions.

Experimentally, since the ME coefficient is a third-rank product tensor property, its value is highly anisotropic and dependent on shape.^{64–66} For example, considering BFO-CFO VANs, the (001)-oriented one has the largest ME coefficient because of its largest piezoelectric constant d_{33} .³ Moreover,



on (001) and (011) SrTiO_3 (STO) substrates, rectangular CFO nanopillars and maze-like CFO nanobelts are embedding in a BFO matrix, respectively; whereas on (012) and (013) STO substrate, a mixed CFO nanopillar morphology forms.^{20,54} However, on (111) STO substrate, CFO becomes the matrix phase decorated with triangular BFO nanopillars.^{20,25,54} Because of these various morphologies, the magnetic anisotropy for differently oriented VANs can be controlled via the shape anisotropy contribution.^{3,25}

Arrangement, aspect ratio, and volume fraction effects

In ME VANs consisting of square-shaped CFO rods embedded in a BTO matrix, PF reveals that, while domain structures within rods are relatively simple, hierarchical ultrafine nanodomains are formed in the ferroelectric matrix (see Figure 2c).⁶⁷ There is thus an extremely high density of domain walls that are susceptible to an externally applied H , leading to a high ME effect (see Figure 2d).⁶⁷ It has also been shown that, with maintaining the shapes and volume fraction of magnetic rods, the distribution of constituent phase, or the geometrical arrangement (square, honeycomb, and triangular arrays) of rods, strongly affects the final domain configuration

(domain wall density) and thus the ME coefficient.⁶⁷

PF can also be used to simulate ME VANs with periodically aligned cuboid-shaped CFO inclusions embedded in a BTO matrix.⁶⁸ By changing the aspect ratio, $r=c/a$, of the cuboids, the effects of phase connectivity on the ME coefficient can be systematically considered.⁶⁸ It has been shown that both ME charge and voltage coefficients are significantly larger at large values of r , where the highest values are obtained at magnetic phase fractions of $\sim 65\%$ and $\sim 93\%$, respectively.⁶⁸

Experimentally, the deposition conditions of epitaxial growth (e.g., target volume fraction, growth temperature, growth rate, and gas pressure for PLD) control the stoichiometry,^{56,57} pillar shape,⁵⁸ pillar size,⁵⁹ and pillar distance.⁶⁹

The target volume fraction of perovskite and spinel phases directly determines the stoichiometry of VANs, which further affects their morphologies, and thus the magnetic anisotropy and ME properties.^{19,34} The rich phase usually becomes the matrix. Accordingly, to achieve enhanced out-of-plane magnetic anisotropy, perovskite-rich targets are preferred.^{25,34} By increasing the volume fraction of the pillar phase,

the pillar distance decreases, which affects the coupling effect between the nanopillars.^{23,69}

Other deposition parameters work together to control the growth kinetics, contributing to the stoichiometry, morphology, and properties of VANs.^{19,56} For example, higher growth temperatures and slower growth rates benefit the diffusion process, and thus result in large pillar sizes.¹⁹ The pillar size, on the other hand, affects the coupling behavior amongst the pillars, and the coupling behaviors between pillars and matrices.^{25,58,59,70}

Substrate constraint effects

When simulating thin films, due to the presence of the substrate, more parameters need to be considered. The ME effect in epitaxial ME VANs can also be investigated by PF that takes into account the substrate constraint and the long-range magnetic, electric, and elastic interactions.⁷¹⁻⁷³ It has been suggested that the direction of applied H and the morphology of VANs strongly affect the magnetic-field-induced electric polarization (MIEP).⁷¹ It has also been shown that the MIEP is strongly dependent on the film thickness and the substrate constraints.^{71,72} The highly heterogeneous vertical stress field

suggests that besides the lateral misfit strains between the film and substrate, the vertical strains between the ferroelectric and ferromagnetic phases may also play an important role in determining the ME effects.⁷² In fact, the lateral strain is important when the film thickness is below the critical thickness (a few tens of nanometers). The strain status in VANs is dominated by the vertical lattice coupling if the film is thicker than the critical thickness.^{74,75} For example, magnetic anisotropy and ferroelectricity in thick VANs are dominantly controlled by the vertical strain.

Experimentally, although self-assembled VANs greatly reduce the clamping effect from substrates, the epitaxial strain with the substrate can still modify the VANs' morphology.^{60,63} For example, the diverse morphologies of BFO-CFO VANs on (011) DyScO₃ (DSO), (001) STO, and (011) NdGaO₃ (NGO) lead to unique magnetic anisotropy.⁶¹ Moreover, the selection of (001) LaAlO₃ (LAO) as a substrate, with a dramatic lattice mismatch with BFO, can induce crystal structure changes in BFO, forming a stable tetragonal-like (T-like) phase that can still be self-assembled with CFO in spite of the enhanced vertical strains.^{60,62,76} Interestingly, it has been reported in (001) T-like BFO matrix that the CFO nanopillars are (111) oriented

octahedrons, and consequently, have a unique magnetic anisotropy compared to normal (001) CFO nanopillars embedded in a rhombohedral-like (R-like) BFO matrix, due to the magnetocrystalline anisotropy.^{60,62}

Piezoelectric single crystals (e.g., PMN-PT) have been used as substrates to deposit ME VANs.^{24,26,30} Due to the outstanding piezoelectric property of the substrate, the ME coefficient of BFO-CFO/PMN-PT system can reach 1.3×10^{-7} s/m, which is about three orders of magnitude larger than BFO-CFO/STO VANs.^{30,77,78} Moreover, the magnetization changes exhibit a characteristic “butterfly-like” curves (see **Figure 3a**), demonstrating the feasibility to reversibly obtain multiple non-volatile magnetic states (i.e., more than four stable states in **Figure 3b**).^{24,26,30}

Potentials in devices and applications

Because of the interaction between magnetic and electric order parameters, the characteristic properties of ME VANs (magnetizations, magnetic anisotropy, polarizations, and ME coefficients) are all tunable by applying H and/or E.^{4,7,29} This tunability imparts to ME VANs the potential to be used as active microelectronics.^{4,7,24,79} Some ME VANs have been proposed

for memory and logic devices, taking advantages of their unique nanopillar structures and orientations.^{24,30,80}

Recently, periodic ME VANs have also been reported to fulfill some industrial application demands.^{81,82}

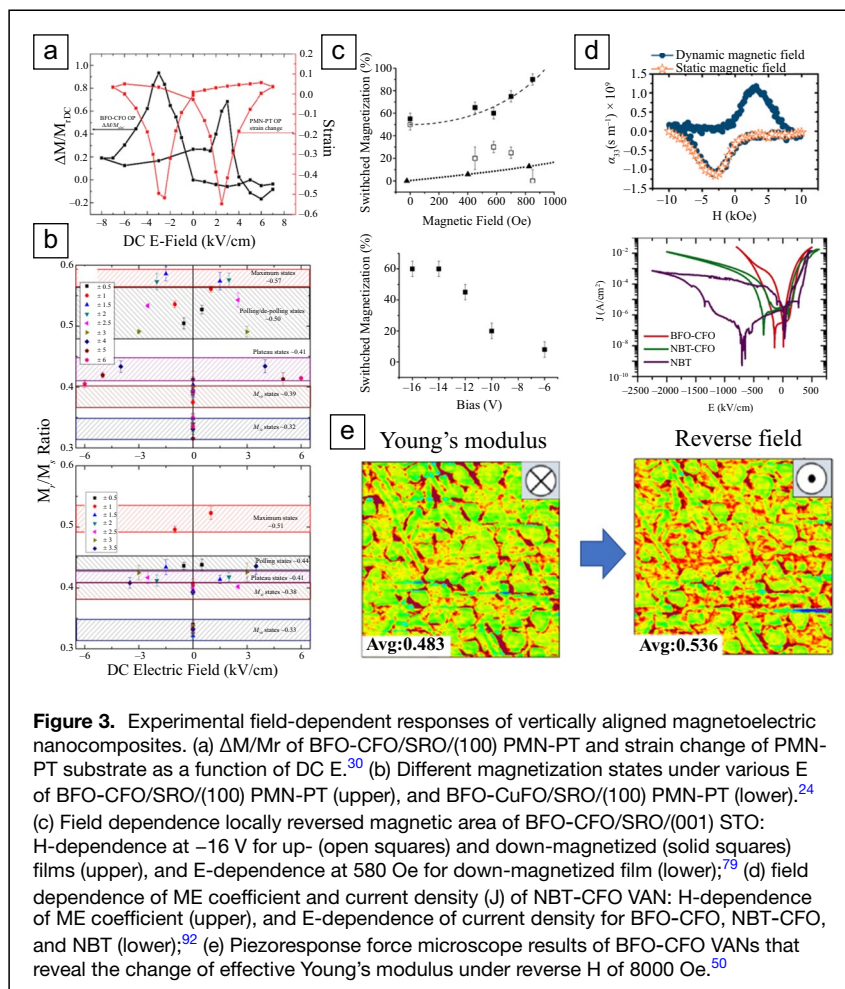
Tunable electronics

The tunability of ME materials have been studied for various applications, such as sensors,^{83,84} converters,^{85,86} and gyrators.^{8,87,88} Although most of these studies use bulk ME composites, researchers are trying hard to achieve the same functionalities in ME thin films, in order to integrate them with silicon-based microelectronics.^{4,7,24,79}

Progress has been realized in ME thin films for sensors,⁸⁹ tunable inductors,⁹⁰ and antennas.⁹¹ Going forward, considering their larger ME coefficients, ME VANs offer more promise than ME thin films.

Memory devices

The field-dependent nature of the ME VANs makes them a promising candidate for next-generation memory devices. Both the E-controlled ME random access memory (MeRAM) and resistant memory (memristor) have been proposed.^{79,92} **Figure 3c** shows for BFO-CFO VAN



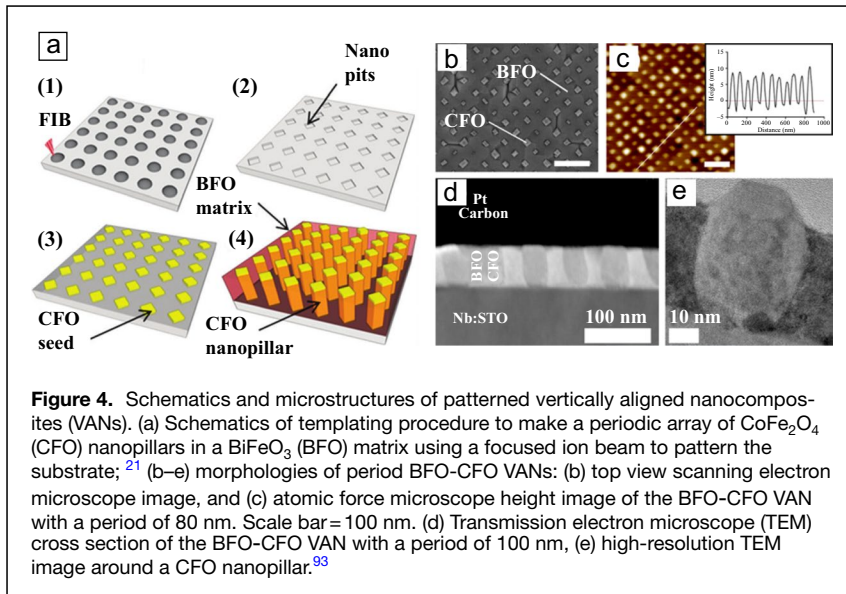


Figure 4. Schematics and microstructures of patterned vertically aligned nanocomposites (VANs). (a) Schematics of templating procedure to make a periodic array of CoFe_2O_4 (CFO) nanopillars in a BiFeO_3 (BFO) matrix using a focused ion beam to pattern the substrate;²¹ (b–e) morphologies of period BFO-CFO VANs: (b) top view scanning electron microscope image, and (c) atomic force microscope height image of the BFO-CFO VAN with a period of 80 nm. Scale bar = 100 nm. (d) Transmission electron microscope (TEM) cross section of the BFO-CFO VAN with a period of 100 nm, (e) high-resolution TEM image around a CFO nanopillar.⁹³

that the local magnetization can be gradually switched with increasing H and E , respectively.⁷⁹ Figure 3d shows for the $\text{Na}_{0.5}\text{Bi}_{0.5}\text{TiO}_3\text{-CoFe}_2\text{O}_4$ (NBT-CFO) VAN that the ME coefficient and resistance are adjustable with fields.⁹² Figure 3e shows for BFO-CFO VANs that the effective Young's modulus measured by piezoresponse force microscope (PFM) are tunable by reverse H .⁵⁰

By depositing ME VANs on piezoelectric PMN-PT substrates, in addition to enhancing their ME coefficient, non-volatility has been reported to provide access to multiple ($N > 2$) remnant states.^{24,30} Accordingly, ME VANs on PMN-PT have been suggested as multilevel cell (MLC) memories, where each single cell can store more than a single binary bit. Such nonbinary memories offer an approach to much higher storage density and a much lower cost-per-bit.²⁴ By varying the binary input values (both H and E), more than four magnetic outputs can be obtained (see Figure 3b). Such multilevel nonvolatile states have been reported for both BFO-CFO VANs and BFO-CuFO VANs on PMN-PT substrates, even though both PMN-PT and CFO/CuFO have volatile properties.²⁴

To use the geometry advantage of the VAN structure to the maximum, each individual nanopillar could naturally be treated as a basic memory element. But a challenge is the partially controllable nanopillar distribution by self-assembly.

Patterned ME VANs

To improve the control of the phase distribution in ME VANs, lithography and seeding techniques have been explored to generate templates and to assist in the growth of ordered/patterned ME VANs.^{19–21,74,93–96} Figure 4a shows a schematic of a templating procedure for ordered periodic CFO nanopillars in a BFO matrix.²¹ Figure 4b–e shows the detailed morphologies of well-ordered BFO-CFO VANs made by such a templating

procedure.⁹³ Experiments have demonstrated notable ME effects in such patterned ME VANs.⁹³

Other templating methods include using electron beam lithography (EBL) to pattern the CFO nucleation sites,⁹⁷ porous anodic aluminum oxide (AAO) film as a mask to pattern hexagonal CFO,^{35,98} and self-assembled triblock terpolymer to guide the self-assembly of VANs.⁹⁵

To simplify the processing and reduce the contamination, VANs with spontaneous ordering have also been reported. A systematic review can be found in Reference 99. Although the spontaneous ordering self-assembly requires much stricter material and substrate selections, it is promising to be adopted in the ordered ME VAN fabrication.

Summary and outlook

ME VANs are attractive due to unique phase distribution morphologies and enhanced strain-mediated ME properties, which provide abundant application potential in microelectronics. PF simulations have been developed to explain and predict the phase distribution and interaction behaviors in ME VANs, leading to several feasible experimental approaches, including shape and orientation adjustments, deposition condition optimizations, and material/substrate selections, to modify and improve the final properties. Consequently, more applications and devices such as tunable electronics and memory devices are proposed based on ME VANs. However, there are still many challenges and opportunities such as (1) achieving higher ME coefficients in ME VANs; (2) understanding the ME effect in ME VANs from a more fundamental level; (3) designing real micro-/nano-electronic devices using ME VANs; (4) utilizing individual nanopillars as the basic electronic component; and (5) developing more convenient methods to produce ordered ME VANs. We hope the previously discussion can help readers to capture key issues in this field.

Acknowledgments

M.G. would like to acknowledge Qishan Scholar Financial Support from Fuzhou University (GXRC-20099); D.V. would like to acknowledge the financial support by the US Department of Energy (DE-FG02-06ER46290) and the Air Force Office of Scientific Research (FA9550-16-1-0001) for various aspects of this research; Y.Y. and W.R. would like to thank the support from the National Science Foundation of China (Grant No. 51831010 and No. 11474167), the Key R&D Program of Shandong (No. 2019QYTPY057), and the Innovation Team Project of Ji'nan (No. 2019GXRC035).

Conflict of interest

On behalf of all authors, the corresponding author states that there is no conflict of interest.

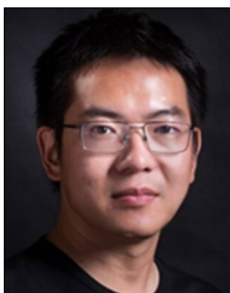
References

- W. Eerenstein, N.D. Mathur, J.F. Scott, *Nature* **442**, 759 (2006)
- N.C.W. Nan, M.I. Bichurin, S. Dong, D. Viehland, G. Srinivasan, *J. Appl. Phys.* **103**, 031101 (2008)
- L. Yan, Z. Wang, Z. Xing, J. Li, D. Viehland, *J. Appl. Phys.* **107**, 064106 (2010)
- C.M. Leung, J. Li, D. Viehland, X. Zhuang, *J. Phys. D* **51**, 263002 (2018)
- D.H. Kim, S. Ning, C.A. Ross, *J. Mater. Chem. C* **7**, 9128 (2019)
- Y. Bitla, Y.-H. Chu, *J. Phys. D* **51**, 234006 (2018)
- X. Liang, C. Dong, H. Chen, J. Wang, Y. Wei, M. Zaeimbashi, Y. He, A. Matyushov, C. Sun, N. Sun, *Sensors* **20**, 1532 (2020)
- J. Zhai, J. Gao, C. De Vreugd, J. Li, D. Viehland, A.V. Filippov, M.I. Bichurin, D.V. Drodzov, G.A. Semenov, S.X. Dong, *Euro. Phys. J. B* **71**, 383 (2009)
- H. Schmid, *Ferroelectrics* **161**, 1 (1994)
- J.P. Rivera, *Ferroelectrics* **161**, 165 (1994)
- G. Lawes, G. Srinivasan, *J. Phys. D* **44**, 243001 (2011)
- M. Fiebig, *J. Phys. D* **38**, R123 (2005)
- R. Ramesh, N.A. Spaldin, *Nat. Mater.* **6**, 21 (2007)
- J. Ma, J. Hu, Z. Li, C.-W. Nan, *Adv. Mater.* **23**, 1062 (2011)
- Y. Wang, J. Hu, Y. Lin, C.-W. Nan, *NPG Asia Mater.* **2**, 61 (2010)
- H. Zheng, J. Wang, S.E. Lofland, Z. Ma, L. Mohaddes-Ardabili, T. Zhao, L. Salamanca-Riba, S.R. Shinde, S.B. Ogale, F. Bai, D. Viehland, Y. Jia, D.G. Schlom, M. Wuttig, A. Roytburd, R. Ramesh, *Science* **303**, 661 (2004)
- L. Yan, Y. Yang, Z. Wang, Z. Xing, J. Li, D. Viehland, *J. Mater. Sci.* **44**, 5080 (2009)
- H. Zheng, J. Wang, L. Mohaddes-Ardabili, M. Wuttig, L. Salamanca-Riba, D.G. Schlom, R. Ramesh, *Appl. Phys. Lett.* **85**, 2035 (2004)
- H. Zheng, F. Straub, Q. Zhan, P.L. Yang, W.K. Hsieh, F. Zavaliche, Y.H. Chu, U. Dahmen, R. Ramesh, *Adv. Mater.* **18**, 2747 (2006)
- H. Zheng, Q. Zhan, F. Zavaliche, M. Sherburne, F. Straub, M.P. Cruz, L.-Q. Chen, U. Dahmen, R. Ramesh, *Nano Lett.* **6**, 1401 (2006)
- T.C. Kim, S. Ojha, G. Tian, S.H. Lee, H.K. Jung, J.W. Choi, L. Kornblum, F.J. Walker, C.H. Ahn, C.A. Ross, D.H. Kim, *J. Mater. Chem. C* **6**, 5552 (2018)
- Y. Li, Z. Wang, J. Yao, T. Yang, Z. Wang, J.-M. Hu, C. Chen, R. Sun, Z. Tian, J. Li, L.-Q. Chen, D. Viehland, *Nat. Commun.* **6**, 6680 (2015)
- Y.-H. Hsieh, J.-M. Liou, B.-C. Huang, C.-W. Liang, Q. He, Q. Zhan, Y.-P. Chiu, Y.-C. Chen, Y.-H. Chu, *Adv. Mater.* **24**, 4564 (2012)
- X. Tang, M. Gao, C.M. Leung, H. Luo, J. Li, D. Viehland, *Appl. Phys. Lett.* **114**, 242903 (2019)
- Z. Wang, Y. Li, R. Viswan, B. Hu, V.G. Harris, J. Li, D. Viehland, *ACS Nano* **7**, 3447 (2013)
- X. Tang, C.M. Leung, M. Gao, C. Winkler, H. Luo, J. Li, D. Viehland, *J. Am. Ceram. Soc.* **102**, 5192 (2019)
- D.H. Kim, X.Y. Sun, N.M. Aimon, J.J. Kim, M.J. Champion, H.L. Tuller, L. Kornblum, F.J. Walker, C.H. Ahn, C.A. Ross, *Adv. Funct. Mater.* **25**, 3091 (2015)
- X. Tang, M. Gao, J. Li, D. Viehland, *J. Appl. Phys.* **126**, 123905 (2019)
- W. Zhang, R. Ramesh, J.L. MacManus-Driscoll, H. Wang, *MRS Bull.* **40**, 736 (2015)
- X. Tang, R. Viswan, M. Gao, C.M. Leung, C. Folger, H. Luo, B. Howe, J. Li, D. Viehland, *Sci. Rep.* **8**, 1628 (2018)
- L. Yan, Z. Xing, Z. Wang, T. Wang, G. Lei, J. Li, D. Viehland, *Appl. Phys. Lett.* **94**, 192902 (2009)
- J. Li, I. Levin, J. Slutsker, V. Provenzano, P.K. Schenck, R. Ramesh, J. Ouyang, A.L. Roytburd, *Appl. Phys. Lett.* **87**, 072909 (2005)
- C.Y. Tsai, H.R. Chen, F.C. Chang, W.C. Tsai, H.M. Cheng, Y.H. Chu, C.H. Lai, W.F. Hsieh, *Appl. Phys. Lett.* **102**, 132905 (2013)
- J.-G. Wan, Y. Weng, Y. Wu, Z. Li, J.-M. Liu, G. Wang, *Nanotechnology* **18**, 465708 (2007)
- X. Gao, B.J. Rodriguez, L. Liu, B. Birajdar, D. Pantel, M. Ziese, M. Alexe, D. Hesse, *ACS Nano* **4**, 1099 (2010)
- Q. Zhan, R. Yu, S.P. Crane, H. Zheng, C. Kisielowski, R. Ramesh, *Appl. Phys. Lett.* **89**, 172902 (2006)
- L. Li, L. Lu, D. Zhang, R. Su, G. Yang, J. Zhai, Y. Yang, *ACS Appl. Mater. Interfaces* **8**, 442 (2016)
- N.M. Aimon, D.H. Kim, H.K. Choi, C.A. Ross, *Appl. Phys. Lett.* **100**, 092901 (2012)
- T.C. Kim, S.H. Lee, H.K. Jung, Y.E. Kim, J.W. Choi, D. Yang, D.H. Kim, *J. Magn. Mater.* **471**, 116 (2019)
- D.P. Kumah, J.H. Ngai, L. Kornblum, *Adv. Funct. Mater.* **30**, 1901597 (2020)
- A.G. Khachatryan, *Phys. Status Solidi B* **35**, 119 (1969)
- A. Khachatryan, G. Shatalov, *Soviet Phys. JETP* **29**, 557 (1969)
- Y. Ni, L. He, A.G. Khachatryan, *J. Appl. Phys.* **108**, 023504 (2010)
- A. Artemev, J. Slutsker, A.L. Roytburd, *Acta Mater.* **53**, 3425 (2005)
- J. Slutsker, A. Artemev, A. Roytburd, *Phys. Rev. Lett.* **100**, 087602 (2008)
- Y. Ni, W. Rao, A.G. Khachatryan, *Nano Lett.* **9**, 3275 (2009)
- A. Chen, Q. Su, H. Han, E. Enriquez, Q. Jia, *Adv. Mater.* **31**, 1803241 (2019)
- M. Rafique, A. Herklotz, K. Dörr, S. Manzoor, *Appl. Phys. Lett.* **110**, 202902 (2017)
- G. Tian, S. Ojha, S. Ning, X. Gao, C.A. Ross, *Adv. Electron. Mater.* **5**, 1900012 (2019)
- L. Wang, J. Bian, L. Lu, Z. Liang, D. Zhang, B. Yang, L. Li, G. Lu, Y. Yang, *J. Mater. Chem. C* **8**, 3527 (2020)
- A. Chen, Y. Dai, A. Eshghinejad, Z. Liu, Z. Wang, J. Bowlan, E. Knall, L. Civale, J.L. MacManus-Driscoll, A.J. Taylor, R.P. Prasankumar, T. Lookman, J. Li, D. Yarotski, Q. Jia, *Adv. Sci.* **6**, 1901000 (2019)
- C. Schmitz-Antoniak, D. Schmitz, P. Borisov, F.M.F. de Groot, S. Stienen, A. Warland, B. Krumme, R. Feyerherm, E. Dudzik, W. Kleemann, H. Wende, *Nat. Commun.* **4**, 2051 (2013)
- D.H. Kim, N.M. Aimon, X. Sun, C.A. Ross, *Adv. Funct. Mater.* **24**, 2334 (2014)
- L. Yan, F. Bai, J. Li, D. Viehland, *J. Am. Ceram. Soc.* **92**, 17 (2009)
- P.P. Wu, X.Q. Ma, J.X. Zhang, L.Q. Chen, *Philos. Mag.* **90**, 125 (2010)
- N. Dix, R. Muralidharan, J.M. Caicedo, D. Hrabovsky, I. Fina, L. Fàbrega, V. Skumryev, M. Varela, J. Guyonnet, P. Paruch, F. Sánchez, J. Fontcuberta, *J. Magn. Mater.* **321**, 1790 (2009)
- N. Dix, R. Muralidharan, B. Warot-Fonrose, M. Varela, F. Sánchez, J. Fontcuberta, *Chem. Mater.* **21**, 1375 (2009)
- D.H. Kim, N.M. Aimon, C.A. Ross, *APL Mater.* **2**, 081101 (2014)
- T. Amrillah, Y.-X. Chen, M.N. Duong, W. Abdussalam, F.M. Simanjuntak, C.-H. Chen, Y.-H. Chu, J.-Y. Juang, *CrystEngComm* **22**, 435 (2020)
- N. Dix, R. Muralidharan, J.-M. Rebled, S. Estradé, F. Peiró, M. Varela, J. Fontcuberta, F. Sánchez, *ACS Nano* **4**, 4955 (2010)
- S.-C. Liao, P.-Y. Tsai, C.-W. Liang, H.-J. Liu, J.-C. Yang, S.-J. Lin, C.-H. Lai, Y.-H. Chu, *ACS Nano* **5**, 4118 (2011)
- T. Amrillah, S.K. Vandurangi, Y. Bitla, T.H. Do, S.-C. Liao, C.-Y. Tsai, Y.-Y. Chin, Y.-T. Liu, M.-L. Lin, Q. He, H.-J. Lin, H.-Y. Lee, C.-H. Lai, E. Arenholz, J.-Y. Juang, Y.-H. Chu, *Nanoscale* **8**, 8847 (2016)
- J. Huang, J.L. MacManus-Driscoll, H. Wang, *J. Mater. Res.* **32**, 4054 (2017)
- G. Jian, C.P. Wong, *AIP Adv.* **7**, 075307 (2017)
- S. Srinivas, J.Y. Li, *Acta Mater.* **53**, 4135 (2005)
- H.Q. Shen, Y.G. Wang, D. Xie, J.H. Cheng, *J. Alloys Compd.* **610**, 11 (2014)
- L. Van Lich, T. Shimada, K. Miyata, K. Nagano, J. Wang, T. Kitamura, *Appl. Phys. Lett.* **107**, 232904 (2015)
- T.N. Yang, J.-M. Hu, C.W. Nan, L.Q. Chen, *Appl. Phys. Lett.* **104**, 052904 (2014)
- Y.-J. Chen, Y.-H. Hsieh, S.-C. Liao, Z. Hu, M.-J. Huang, W.-C. Kuo, Y.-Y. Chin, T.-M. Uen, J.-Y. Juang, C.-H. Lai, H.-J. Lin, C.-T. Chen, Y.-H. Chu, *Nanoscale* **5**, 4449 (2013)
- N.M. Aimon, J. Liao, C.A. Ross, *Appl. Phys. Lett.* **101**, 232901 (2012)
- J.X. Zhang, Y.L. Li, D.G. Schlom, L.Q. Chen, F. Zavaliche, R. Ramesh, Q.X. Jia, *Appl. Phys. Lett.* **90**, 052909 (2007)
- H.T. Chen, L. Hong, A.K. Soh, *J. Appl. Phys.* **109**, 094102 (2011)
- X. Lu, H. Li, B. Wang, *J. Mech. Phys. Solids* **59**, 1966 (2011)
- J.L. MacManus-Driscoll, P. Zerrer, H. Wang, H. Yang, J. Yoon, A. Fouchet, R. Yu, M.G. Blamire, Q. Jia, *Nat. Mater.* **7**, 314 (2008)
- A. Chen, J.-M. Hu, P. Lu, T. Yang, W. Zhang, L. Li, T. Ahmed, E. Enriquez, M. Weigand, Q. Su, H. Wang, J.-X. Zhu, J.L. MacManus-Driscoll, L.-Q. Chen, D. Yarotski, Q. Jia, *Sci. Adv.* **2**, e1600245 (2016)
- M. Gao, R. Viswan, X. Tang, C.M. Leung, J. Li, D. Viehland, *Sci. Rep.* **8**, 323 (2018)
- F. Zavaliche, H. Zheng, L. Mohaddes-Ardabili, S.Y. Yang, Q. Zhan, P. Shafer, E. Reilly, R. Chopdekar, Y. Jia, P. Wright, D.G. Schlom, Y. Suzuki, R. Ramesh, *Nano Lett.* **5**, 1793 (2005)
- M. Gao, C. Luo, W.-Y. Chang, C.M. Leung, J. Tian, J. Li, X. Jiang, D. Viehland, *Acta Mater.* **169**, 28 (2019)
- F. Zavaliche, T. Zhao, H. Zheng, F. Straub, M.P. Cruz, P.L. Yang, D. Hao, R. Ramesh, *Nano Lett.* **7**, 1586 (2007)
- S.A. Wolf, J. Lu, M.R. Stan, E. Chen, D.M. Treger, *Proc. IEEE* **98**, 2155 (2010)
- S.M. Stratulat, X. Lu, A. Morelli, D. Hesse, W. Erfurth, M. Alexe, *Nano Lett.* **13**, 3884 (2013)
- G. Tian, F. Zhang, J. Yao, H. Fan, P. Li, Z. Li, X. Song, X. Zhang, M. Qin, M. Zeng, Z. Zhang, J. Yao, X. Gao, J. Liu, *ACS Nano* **10**, 1025 (2016)
- Y. Wang, D. Gray, D. Berry, J. Gao, M. Li, J. Li, D. Viehland, *Adv. Mater.* **23**, 4111 (2011)
- J. Gao, D. Gray, Y. Shen, J. Li, D. Viehland, *Appl. Phys. Lett.* **99**, 153502 (2011)
- Y. Zhou, Y. Yan, S. Priya, *Appl. Phys. Lett.* **104**, 232906 (2014)
- Y. Wang, X. Zhao, W. Di, H. Luo, S.W. Or, *Appl. Phys. Lett.* **95**, 143503 (2009)
- X. Zhuang, C.M. Leung, J. Li, D. Viehland, *AIP Adv.* **8**, 056607 (2017)
- C.M. Leung, X. Zhuang, J. Xu, G. Srinivasan, J. Li, D. Viehland, *Appl. Phys. Lett.* **109**, 202907 (2016)
- T. Nan, Y. Hui, M. Rinaldi, N.X. Sun, *Sci. Rep.* **3**, 1985 (2013)

90. H. Lin, T. Nan, Q. Zhenyun, Y. Gao, Y. Hui, X. Wang, R. Guo, A. Belkessam, S. Wei, M. Rinaldi, N.X. Sun, in 2016 IEEE MTT-S International Microwave Symposium (IMS) (2016), p. 1.
91. T. Nan, H. Lin, Y. Gao, A. Matyushov, G. Yu, H. Chen, N. Sun, S. Wei, Z. Wang, M. Li, X. Wang, A. Belkessam, R. Guo, B. Chen, J. Zhou, Z. Qian, Y. Hui, M. Rinaldi, M.E. McConney, B.M. Howe, Z. Hu, J.G. Jones, G.J. Brown, N.X. Sun, *Nat. Commun.* **8**, 296 (2017)
92. R. Wu, A. Kursumovic, X. Gao, C. Yun, M.E. Vickers, H. Wang, S. Cho, J.L. MacManus-Driscoll, *ACS Appl. Mater. Interfaces* **10**, 18237 (2018)
93. N.M. Aimon, D.H. Kim, X. Sun, C.A. Ross, *ACS Appl. Mater. Interfaces* **7**, 2263 (2015)
94. M. Fan, B. Zhang, H. Wang, J. Jian, X. Sun, J. Huang, L. Li, X. Zhang, H. Wang, *Adv. Mater.* **29**, 1606861 (2017)
95. H.K. Choi, N.M. Aimon, D.H. Kim, X.Y. Sun, J. Gwyther, I. Manners, C.A. Ross, *ACS Nano* **8**, 9248 (2014)
96. N.M. Aimon, H.K. Choi, X.Y. Sun, D.H. Kim, C.A. Ross, *Adv. Mater.* **26**, 3063 (2014)
97. R. Comes, H. Liu, M. Khokhlov, R. Kasica, J. Lu, S.A. Wolf, *Nano Lett.* **12**, 2367 (2012)
98. X. Lu, Y. Kim, S. Goetze, X. Li, S. Dong, P. Werner, M. Alexe, D. Hesse, *Nano Lett.* **11**, 3202 (2011)
99. X. Sun, J.L. MacManus-Driscoll, H. Wang, *Annu. Rev. Mater. Res.* **50**, 229 (2020) □



Min Gao is a lecturer in the College of Materials Science and Engineering at Fuzhou University, China. He obtained his PhD degree in materials science and engineering in 2019 from the Virginia Polytechnic Institute and State University. His research interests include magnetoelectric nanocomposites, antiferroelectric thin films, and ferroelectric single crystals. Gao can be reached by email at gaom@fzu.edu.cn.



Yaodong Yang is a professor in the School of Mechanical and Automotive Engineering at Qilu University of Technology (Shandong Academy of Sciences), China. He obtained his PhD degree from Virginia Polytechnic Institute and State University, and a bachelor's degree from Zhejiang University, China. His research interests include using advanced experimental methods such as machine learning to design and fabricate smart materials and building new smart systems. He has published approximately 85 papers and has an H-index of 18. He is a board member of *Scientific Reports*. Yaodong can be reached by email at yaodongy@qlu.edu.cn.



Wei-Feng Rao is a professor in the Department of Materials Processing at Qilu University of Technology, China. He obtained his PhD degree in materials science and engineering at the Virginia Polytechnic Institute and State University. His research interests include the microstructure formation and property prediction of phase-transforming materials. Rao can be reached by email at wfrao@qlu.edu.cn.



Dwight Viehland is the Jack E. Cowling Professor of Engineering in the Department of Materials Science and Engineering at the Virginia Polytechnic Institute and State University. He obtained his PhD degree in solid-state science at The Pennsylvania State University. His research interests include electrical, magnetic, and structural properties of oxides. He has published extensively on magnetoelectric materials, phase transformations, domain structures in ferroelectrics, and epitaxial deposition of all oxide heterostructures. He has published more than 500 papers, which have received approximately 39,000 citations (Google Scholar). He is a Fellow of The American Ceramic

Society, and was an Office of Naval Research Young Investigator. Viehland can be reached by email at dviehlan@vt.edu.